THE JOURNAL OF PHYSICAL CHEMISTRY B
A JOURNAL OF THE AMERICAN CHEMICAL SOCIETY

pubs.acs.org/JPCB

Article

Phase Behavior and Electrochemical Properties of Highly Asymmetric Redox Coacervates

Lucy L. Coria-Oriundo, Gabriel Debais, Eugenia Apuzzo, Santiago E. Herrera,* Marcelo Ceolín, Omar Azzaroni, Fernando Battaglini, and Mario Tagliazucchi*

Cite This: *J. Phys. Chem. B* 2023, 127, 7636–7647

Read Online

ACCESS | Metrics & More | Article Recommendations | Supporting Information

ABSTRACT: This work reports the phase behavior and electrochemical properties of liquid coacervates made of ferricyanide and poly(ethylenimine). In contrast to the typical polyanion/polycation pairs used in liquid coacervates, the ferricyanide/poly(ethylenimine) system is highly asymmetric because poly(ethylenimine) has approximately 170 charges per molecule, while ferricyanide has only 3. Two types of phase diagrams were measured and fitted with a theoretical model. In the first type of diagram, the stability of the coacervate was studied in the plane given by the concentration of poly(ethylenimine) versus the concentration of ferricyanide for a fixed concentration of added monovalent salt (NaCl). The second type of diagram involved the plane given by the concentration of poly(ethylenimine) vs the concentration of the added monovalent salt for a fixed poly(ethyleneimine)/ferricyanide ratio. Interestingly, these phase diagrams displayed qualitative similarities to those of symmetric polyanion/polycation systems, suggesting that coacervates formed by a polyelectrolyte and a small multivalent ion can be treated as a specific case of polyelectrolyte coacervate. The characterization of the electrochemical properties of the coacervate revealed that the addition of monovalent salt greatly enhances charge transport, presumably by breaking ion pairs between ferricyanide and poly(ethylenimine). This finding highlights the significant influence of added salt on the transport properties of coacervates. This study provides the first comprehensive characterization of the phase behavior and transport properties of asymmetric coacervates and places these results within the broader context of the better-known symmetric polyelectrolyte coacervates.

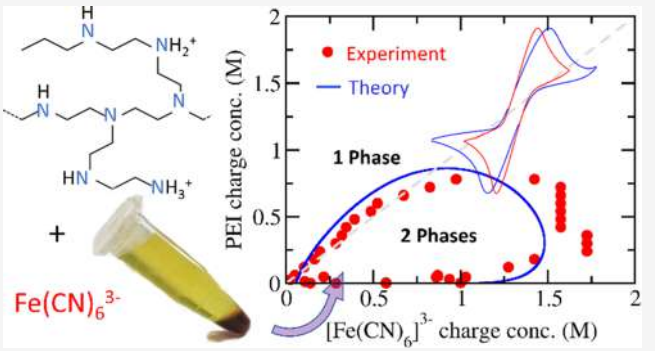

1. INTRODUCTION

Over the past century, there has been extensive research on the phase separation of oppositely charged macromolecules due to weak interactions.[1−8] This field witnessed significant breakthroughs in the 1930s with the work of de Jong and Kruyt who published a series of articles describing what we know today as complex coacervates.[9,10] According to Alexander Oparin's origin of life theory,[6] complex coacervates are defined as solutions of highly concentrated polyelectrolyte complexes that are dispersed in a continuous phase made mostly by water molecules. As coacervates are liquid in nature, they could act as membraneless compartments capable of loading and releasing metabolites, promoting specific chemical reactions, and dynamically modifying their structure without dissolving.[11] Complex coacervates are very interesting materials *per se* since they have an extremely low surface tension[12] and their viscosity depends on the concentration of the salt.[13,14] Early investigations proposed applications in membranes and battery electrolytes[7] due to their good electrical conductivity. More recently, coacervates have been explored as underwater adhesives[15,16] and matrixes for the encapsulation of a wide variety of molecules and biomolecules.[17]

In recent years, it was shown that polyelectrolytes can undergo coacervation not only by interacting with other polyelectrolytes but also by interacting with low-molecular-weight multicharged ions (multivalent ions).[8,18] This class of polyelectrolyte/multivalent-ion complexes and traditional polycation/polyanion coacervates has historically evolved as different research fields.[18−20] However, polyelectrolyte/multivalent-ion complexes can be thought of as a particular case of coacervates, where one of the polyelectrolytes has been replaced by a "short-chain" polyion. While symmetric complex coacervates (*i.e.*, two oppositely charged polyelectrolytes having the same chain lengths, degrees of ionization, and

Received: May 31, 2023
Revised: August 10, 2023
Published: August 28, 2023

concentrations) were thoroughly investigated and their phase diagram is well-characterized,[3,5,21,22] our fundamental understanding of asymmetric coacervates has lagged behind.

In symmetric systems, it is reasonable to assume that the polyanion and polycation will be present in a stoichiometric relationship in both the coacervate and in the dilute phase. This assumption enables a description of the phase diagram in terms of only two degrees of freedom: (1) the total concentration of the polymers and (2) the concentration of the salt (monovalent ions). Therefore, the well-known binodal phase diagram can be constructed by determining these two variables in dilute and concentrated phases.[21,23] This diagram contains relevant information, such as the salt resistance (maximum salt concentration for which liquid−liquid phase separation occurs) and the partition of salt between phases. Moreover, symmetric coacervates were theoretically studied with different approaches, including the random phase approximation,[24−27] field theoretic approaches,[28,29] the PRISM theory,[3] chemical-equilibria approaches,[23,30,31] and computer simulations.[2,21] On the other hand, complex coacervates with some degree of asymmetry (as most real systems are) were less explored. Here, it is important to realize that large asymmetries in chain length or charge per molecule will result in an asymmetric distribution of the macroions within the two phases, even if both macroions were mixed in a stoichiometric ratio. A major contribution to the study of asymmetric complex coacervates was made by Wang and co-workers who investigated both concentration and charge asymmetry using computer simulations and a liquid-state theory.[32,33] Some experimental approaches were also reported; however, these works did not systematically study the effect of concentration.[34]

Asymmetric coacervates made of polyelectrolytes and multivalent ions are appealing systems for a variety of applications. Polyamine-phosphate colloids have been proposed as nanocarriers for drug delivery.[18,35] Coacervates based on charged bio-macromolecules (mostly polylysine, polyarginine, and nucleic acids) and a wide variety of bioactive multivalent ions (such as ATP and other metabolites) have been reported, opening an avenue to the design of bioactive colloidal aggregates.[36,37] In this context, a series of coacervate materials were reported with capacity to be formed and to be dissolved by applying external stimuli,[19,38,39] to load biomolecules,[35] and even to serve as nanoreactors for biologically relevant reactions.[36,40] Considering that the process of asymmetric coacervation localizes a soluble multivalent ion within a new liquid phase through the interaction with a polyelectrolyte, then coacervation can be used as a technique to concentrate a specific multivalent ion and to sequester it selectively. In the case where the multivalent ion is redox-active, this approach allows to create electroactive coacervates. For example, we recently demonstrated that ferricyanide ($z = -3$) and ferrocyanide ($z = -4$) interact with branched poly(ethylenimine) (PEI) to form coacervate droplets that are able to be selectively dissolved (or produced) by multiple stimuli, including pH, ionic strength, and redox agents.[41] Similarly, Spruijt and co-workers combined ferricyanide and ferrocyanide with different cationic peptides to form coacervate droplets with the capacity to spatially localize chemical reactions within the coacervate.[42] In addition to these two examples, the examples in the literature of liquid coacervates made of polyelectrolytes and redox multivalent ions are scarce, and their electrochemical and physical−chemical properties remain mainly unexplored.

In this work, we characterize the phase behavior, physical−chemical, and electrochemical properties of ferricyanide/poly(ethylenimine) liquid coacervates. We choose this particular system in order to shed light on two scarcely explored physical−chemical phenomena: (i) the role of asymmetry in the phase behavior of coacervates and (ii) the electrochemical behavior of redox coacervates. We provide here the first systematic study of the phase behavior of this system by measuring phase diagrams in the planes determined by (i) the concentration of both macroions (at a constant added monovalent salt concentration) and (ii) the total macroion concentration vs. the concentration of added salt (for a stoichiometric relationship between the macroions). To gain fundamental understanding on these results, we developed a theoretical framework based on the chemical-equilibrium approach.[23,30,43] This model can quantitatively fit the two phase diagrams and reveals that the phase diagram in the plane given by the concentration of both macroions is asymmetric. Finally, we demonstrate that the ferricyanide ions within the coacervate are electrochemically addressable and that the apparent diffusion coefficient for charge transport (which determines how fast the redox process is propagated within the coacervate) strongly depends on the concentration of added salt.

2. MATERIALS AND METHODS

2.1. Materials. Coacervates were prepared using branched poly(ethylenimine) (PEI, $M_w \sim 25{,}000$, Sigma-Aldrich) and potassium hexacyanoferrate(III) (Merck). Poly(allylamine hydrochloride) ($M_w \sim 58{,}000$, Sigma-Aldrich) and poly(diallyldimethylammonium chloride) ($M_w \sim 100{,}000$−200,000, 20% wt. solution, Sigma-Aldrich) were used for preliminary assays. All solutions were prepared using Milli-Q water (18.2 MΩ·cm) and the pH was adjusted using concentrated hydrochloric acid (Cicarelli).

2.2. Coacervate Preparation and Construction of the Phase Diagram. For each set of coacervates with fixed PEI concentration, two stock solutions of $Fe(CN)_6^{3-}$ and PEI were prepared and the pH of each solution was adjusted to 6 with HCl. The molar concentration of PEI monomers was calculated using a molar weight of 43 g/mol. Next, the proper amounts of (1) PEI stock solution, (2) water, (3) 3.5 M NaCl, and (4) $Fe(CN)_6^{3-}$ stock solution were placed in a beaker to obtain a solution with the target final concentrations. These mixtures resulted in highly turbid yellow/orange-colored solutions, which were stored overnight to complete the liquid−liquid phase separation (LLPS) process. Although LLPS was commonly observed only a few minutes after mixing, in some cases, it started a few hours after preparation. For the highest concentrations of $Fe(CN)_6^{3-}$ studied, we prepared the stock solutions of this salt at 80 °C in order to increase its solubility. The phase diagram was constructed by observing whether the mixture was phase-separated (red dot) or not (black dot).

2.3. Determination of the Salt Resistance. A series of coacervate samples with no added salt ([NaCl] = 0 M) were prepared, scanning the concentration of PEI between 0 and 2.5 M and fixing the $Fe(CN)_6^{3-}$ concentration in each sample to obtain $[PEI]/[Fe(CN)_6^{3-}] = 6$. Next, aliquots of 3.5 M NaCl solution were added to each sample until it became translucid. The addition of NaCl was made using small aliquots of known

https://doi.org/10.1021/acs.jpcb.3c03680
J. Phys. Chem. B 2023, 127, 7636−7647

volume and shaking the tube before each addition. At the end of the experiment, the final [NaCl] in the sample was calculated.

2.4. Electrochemical Measurements. We prepared coacervates with [PEI] = 0.5 M and [$Fe(CN)_6^{3-}$] = 0.083 M and different concentrations of added NaCl (0, 0.6, and 1.2 M). To facilitate LLPS, the system was centrifuged at 4000*g* for 10 min or until the supernatant was translucent. Then, the supernatant was removed, and the coacervate phase was placed into a three-electrode Teflon cell for electrochemical measurements. Cyclic voltammetry was performed at different scan rates (from 1 to 500 mV/s) with a glassy-carbon working electrode (geometrical area = 0.071 cm^2), a gold-sheet counter electrode, and a Ag/AgCl (KCl 3 M) reference electrode. All electrochemical measurements were carried out with a Gamry potentiostat (Gamry Interface 1000, Gamry Instruments). Electrochemical impedance spectroscopy (EIS) was performed in the coacervates with the same three-electrode setup applying frequencies from 1 Hz to 50 kHz with an amplitude of 10 mV around the apparent redox potential of the $Fe(CN)_6^{3-}$/$Fe(CN)_6^{4-}$ couple. The EIS Spectrum Analyser (EISSA) software (http://www.abc.chemistry.bsu.by/vi/analyser/) was used for data processing.

2.5. Spectrophotometric Measurements. UV−visible spectra were recorded using an Ocean Optics diode array instrument and the data was processed using SpectraSuite software. All experiments were performed using cuvettes with a 1 cm optical path and at room temperature. $Fe(CN)_6^{3-}$ concentration in the coacervate phase (required to calculate D and k^0) was determined by ultraviolet−visible (UV−vis) spectroscopy. First, an aliquot of 50 μL was carefully taken from the coacervate phase. Then, the coacervate aliquot was placed in a beaker containing 1 M NaCl until complete dissolution and transferred to a 50 mL volumetric flask (volume was completed with 1 M NaCl). The absorbance of the final solution was measured at 420 nm (optical density between 0.3 and 0.5) and the concentration of $Fe(CN)_6^{3-}$ was calculated by means of the molar extinction coefficient of $Fe(CN)_6^{3-}$ from the literature.[44]

2.6. Theoretical Methods. The chemical-equilibrium formalism for polyelectrolyte coacervation for the asymmetric case is described in detail in the Supporting Information. We provide here only an outline of its formulation. Briefly, we propose an approximated grand canonical free-energy functional per unit of volume for a homogeneous polyanion/polycation phase

$$\beta\omega = -\frac{S_{trans}}{Vk_B} + \frac{\beta F_{chem}}{V} - \sum_i \beta\mu_i\rho_i \tag{1}$$

where V is the volume of the system, k_B is Boltzmann's constant, and $\beta = 1/k_BT$. The first term in eq 1 results from the translational entropy of all species in the system

$$-\frac{S_{trans}}{Vk_B} = \sum_{s,c^+,a^-} \rho_i[\ln(\rho_i v_s) - 1] + \rho_{MA}[\ln(\rho_{MA} v_s) - 1] + \rho_{MC}[\ln(\rho_{MC} v_s) - 1] \tag{2}$$

where v_s is the volume of the solvent and ρ_i is the number density of species i, i = MA for macroanions ($Fe(CN)_6^{3-}$), MC for macrocation chains (PEI), c^+ and a^- for the monovalent salt anions and cations, and s for the solvent (water).

The second term is the contribution from ion-pairing chemical equilibria. We explicitly consider the following reactions

(i) Macroion−Macroion complexation

$$M\text{-}A^- + M\text{-}C^+ \rightleftarrows [M\text{-}A^- \cdots M\text{-}C^+] \tag{3}$$

and (ii) complexation between macroions and monovalent salt ions

$$M\text{-}A^- + c^+ \rightleftarrows [M\text{-}A^- \cdots c^+] \tag{4}$$

and

$$M\text{-}C^+ + a^- \rightleftarrows [M\text{-}C^+ \cdots a^-] \tag{5}$$

At this point, it is very important to note that these reactions involve the binding of a single association site (*i.e.*, a charged site) in the macroions with either a single association site in the other macroion eq 3 or a monovalent ion in solution (eqs 4 and 5). For example, $Fe[(CN)_6]^{3-}$ has three binding sites. Binding sites are assumed to be independent, and therefore the association constants are insensitive to the state of binding of the neighbor sites. This approximation, which may be refined in future theoretical formulations of our theory, implies that the association constants used in eqs 3−5 should be considered as effective, averaged values.

The free-energy contribution that results from these chemical equilibria is

$$\frac{\beta F_{chem}}{V} = \sum_{i=MA,MC}\left[N_i\rho_i \sum_{j=un\text{-}as,as,as\text{-}ion} f_j^i(\ln(f_j^i) + \beta\mu_j^{o,i})\right] - N_{MA}\rho_{MA}f_{as}^{A}(\ln(N_{MA}\rho_{MA}f_{as}^{MA}v_{as}) - 1) + \sum_{c^+,a^-}\beta\rho_i\mu_j^o \tag{6}$$

(the derivation of this term is explained in detail in refs 23, 45). In this term, N_i (i = MA, MC) is the number of charges per molecule of the macroion i and f_j^i is the fraction of those charges that are in state j, where j = "un-as", (unassociated charge), "as" (charge forming an ion pair with the oppositely charged macroion), or "as-ion" (charge forming an ion pair with an oppositely charged monovalent ion). v_{as} is a volume associated with the macroion/macroion complex, μ_i^o is the standard chemical potential of species i (i = c^+, a^-, s), and $\mu_j^{o,i}$ is the standard chemical potential of a charged site of type i (i = MA, MC for the charged sites in the macroanion and macrocation, respectively) in state j (j = "un-as", "as", or "as-ion"). These standard chemical potentials are directly related to the equilibrium constants of eqs 3−5 (see the Supporting Information).

The final term in eq 1 accounts for the fact that ω is a grand canonical potential (*i.e.*, we fix the chemical potentials of all species rather than their number of particles). The summation over i runs over all chemical species in the system, i = a^+, c^-, MA, MC, and s (and includes small ions associated to the macroions; see the Supporting Information).

Finally, steric repulsions are included into the model using an incompressibility constraint

https://doi.org/10.1021/acs.jpcb.3c03680
J. Phys. Chem. B 2023, 127, 7636−7647

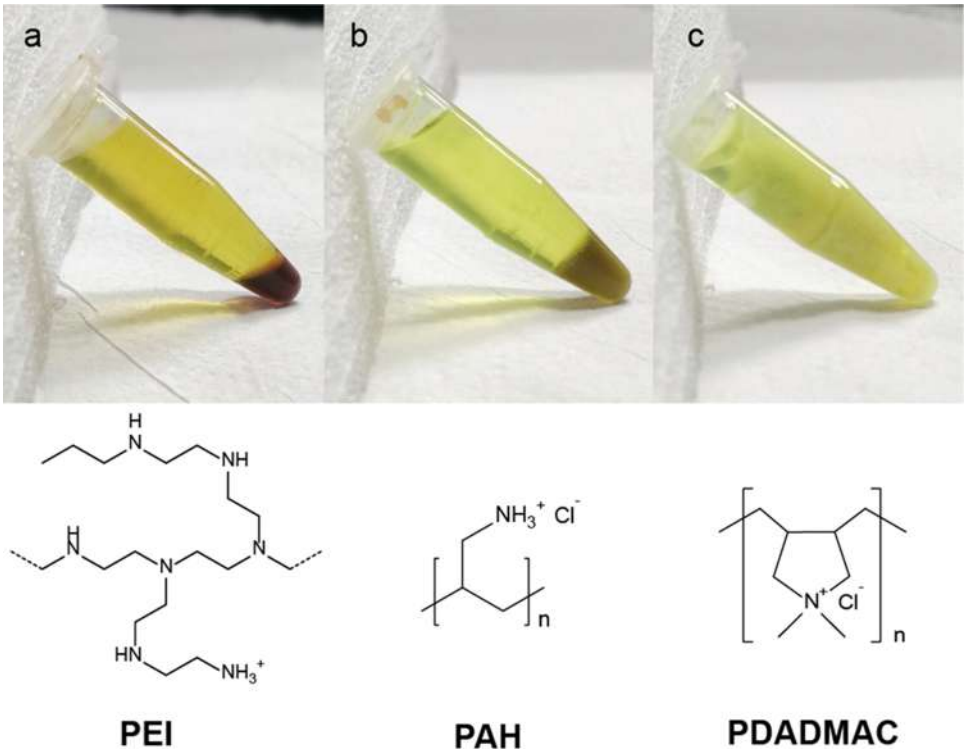

Figure 1. Photographs of vials containing 0.2 M $Fe(CN)_6^{3-}$, 0.5 M NaCl, and 0.6 M polyamine (monomer concentration). Three polyamines were tested: (a) PEI, (b) PAH, and (c) PDADMAC. All samples were stored overnight to allow for the completion of the complexation process. These images were acquired immediately after tilting the tubes to illustrate different fluidities of the concentrated phases.

$$N_{MA}\rho_{MA}v_{MA} + N_{MC}\rho_{MC}v_{MC} + \sum_{i=s,\,c^+,a^-}\rho_i v_i + v_{c^+}(f^{MA}_{as\text{-}ion}N_{MA}\rho_{MA}) + v_{a^-}(f^{MC}_{as\text{-}ion}N_{MC}\rho_{MC}) = 1 \quad (7)$$

where v_i is the volume of the species i (in the case of the macroions, v_{MA} and v_{MC} are the volume per charge, *i.e.*, the total volume of the macroion divided by the number of charges per molecule). Note that the last two terms in the left-hand side account for the volume of the small cations and anions that are bound to the charges in the macroions. Two additional constraints are introduced to enforce the stoichiometry of macroion−macroion pairs and the global electroneutrality of the phase, as discussed in the Supporting Information. The three constraints are enforced using Lagrange multipliers. Notably, the Lagrange multipliers associated with the incompressibility and electroneutrality constraints have the physical meaning of the osmotic pressure and the electrostatic potential of the phase.

In order to calculate the binodal diagram of the system, we first analytically minimize ω (subjected to the three constraints described above) with respect to ρ_i and f^i_j. This procedure yields expressions for (i) the chemical potentials of all species, (ii) the chemical-equilibria reactions (3−5), and (iii) the thermodynamic pressure of the system, $\beta p = -\beta\omega$; see the Supporting Information. Each point along the binodal curve indicates the composition of a phase, for which there is another coexisting phase (with a different composition) that has the same chemical potentials for all species and the same thermodynamic pressure. It is important to note that since we plot only a two-dimensional projection of the entire multidimensional phase diagram, the composition of that coexisting phase does not necessarily lie in the phase diagram, and, therefore tie lines cannot be plotted in this figure; see the discussion below.

3. RESULTS AND DISCUSSION

We first assessed the capacity of $Fe(CN)_6^{3-}$ to form coacervates with polycations by performing preliminary assays mixing aqueous solutions of $Fe(CN)_6^{3-}$ and different polyamines at pH = 6 in the presence of 0.5 M NaCl. Three different polyamines were tested: poly(allylamine hydrochloride) (PAH), branched poly(ethylenimine) (PEI), and poly(diallyldimethylammonium chloride) (PDADMAC). Figure 1 shows that liquid−liquid phase separation (LLPS) was observed only when using PAH and PEI (both weak polyelectrolytes). In the case of PDADMAC (strong polyelectrolyte), a solid-like precipitate was obtained instead of a liquid coacervate.

According to Lutkenhaus et al.,[46,47] the glass transition temperature (T_g) of polyelectrolyte complexes decreases as the content of water molecules surrounding intrinsic ion pairs (*i.e.*, ion pairs between oppositely charged polyelectrolytes) increases.[48] In other words, water molecules are believed to act as plasticizers, weakening intrinsic ion pairs and allowing the sliding motion of polyelectrolyte chains. The content of water molecules within polyelectrolyte complexes and, therefore, the viscoelastic properties of the macroscopic phase, depend on several factors such as the type and concentration of monovalent ions (which break some intrinsic ion pairs, forming salt-ion/polyelectrolyte extrinsic ion pairs),[49] hydrogen bonding,[50] cation−π and π−π interactions,[51,52] hydrophilic/hydrophobic interactions,[53] and polymer rigidity.[54] In PDADMAC/$Fe(CN)_6^{3-}$, PDADMAC is a strong polyelectrolyte and thus has a high linear charge density, which leads to

https://doi.org/10.1021/acs.jpcb.3c03680
J. Phys. Chem. B 2023, 127, 7636−7647

a lowly hydrated complex. On the other hand, PAH is a weak polyelectrolyte and its primary amines are partially protonated. Thus, its linear charge density is smaller than that of PDADMAC, and the PAH/$Fe(CN)_6^{3-}$ complexes are expected to be hydrated. In comparison with the other two complexes, PEI/$Fe(CN)_6^{3-}$ coacervates are highly fluid. Branched PEI contains primary, secondary, and tertiary amino groups in an approximate ratio of 1:2:1.[55] At pH = 6, the protonation degree of PEI is about 0.3 with a low degree of protonated tertiary amines.[56] As $Fe(CN)_6^{3-}$ behaves as an ionic cross-linker rather than as a polyanion, the PEI/$Fe(CN)_6^{3-}$ complex can be thought of as PEI chains interconnected by $Fe(CN)_6^{3-}$ ions. Therefore, the fact that PEI/$Fe(CN)_6^{3-}$ undergoes liquid coacervation instead of forming a solid precipitate suggests that the cross-linking between PEI chains by $Fe(CN)_6^{3-}$ is labile. This weak cross-linking probably results from the low degree of protonation of PEI and its branched nature, which sterically hinders ion-paring interactions and disfavors entanglement, thereby contributing to the fluidity of the coacervate. The focus of this work is to fill current knowledge gaps related to (i) the phase diagrams of highly asymmetric coacervates and (ii) the electrochemical behavior of redox coacervates in the context of potential future applications. Considering the latter goal, we selected PEI/$Fe(CN)_6^{3-}$ for further studies because we expect its fluid nature will maximize the diffusion coefficient of $Fe(CN)_6^{3-}$ and, therefore, its redox reversibility within the coacervate phase.

3.1. Phase Behavior of PEI/$Fe(CN)_6^{3-}$ Coacervates. In order to study the phase behavior of PEI/$Fe(CN)_6^{3-}$ coacervates, we constructed a phase diagram in the [PEI] *vs* [$Fe(CN)_6^{3-}$] plane at a fixed concentration of added NaCl of 0.5 M; see Figure 2a. Briefly, we prepared a series of solutions with varying PEI and $Fe(CN)_6^{3-}$ concentrations and placed a red dot (or a black dot) in the graph if LLPS was (or was not) observed for each solution. The complete phase diagram is shown in Figure 2a in which the area highlighted in orange represents the composition region where LLPS occurs. At this point, it is important to note that (even in a simplified analysis), the composition of each phase will depend on five independent variables. For example, we can consider [PEI], [$Fe(CN)_6^{3-}$], [Na^+], [K^+], and [H^+] as these independent variables (then, the concentration of [Cl^-] can be obtained from global electroneutrality and that of [OH^-] from the water self-dissociation equilibria). In order to reduce the complexity of the problem, we decided to fix [Na^+] = 0.5 M and pH = 6 (which fixes the chemical potential of H^+ rather than its concentration). Moreover, at the onset of LLPS (where the minority phase is vanishingly small and the composition of the majority phase matches the global composition) [K^+] = 3·[$Fe(CN)_6^{3-}$] for the majority phase because of global stoichiometry. These considerations allow to define the composition of the majority phase at the onset of LLPS (binodal line) using the two variables in the plot of Figure 2a ([PEI] and [$Fe(CN)_6^{3-}$]). Therefore, the phase diagram in Figure 2a is a two-dimensional (2D) cut of the full five-dimensional (5D) phase diagram of the system. We stress that the binodal in the phase diagram of Figure 2a indicates only the composition of the majority phase. The composition of the minority phase produced at the onset of LLPS was not measured, but even if such information were available, it would not be correct to plot it in Figure 2a because Na^+, K^+, and Cl^- may partition differently between both phases (in other words,

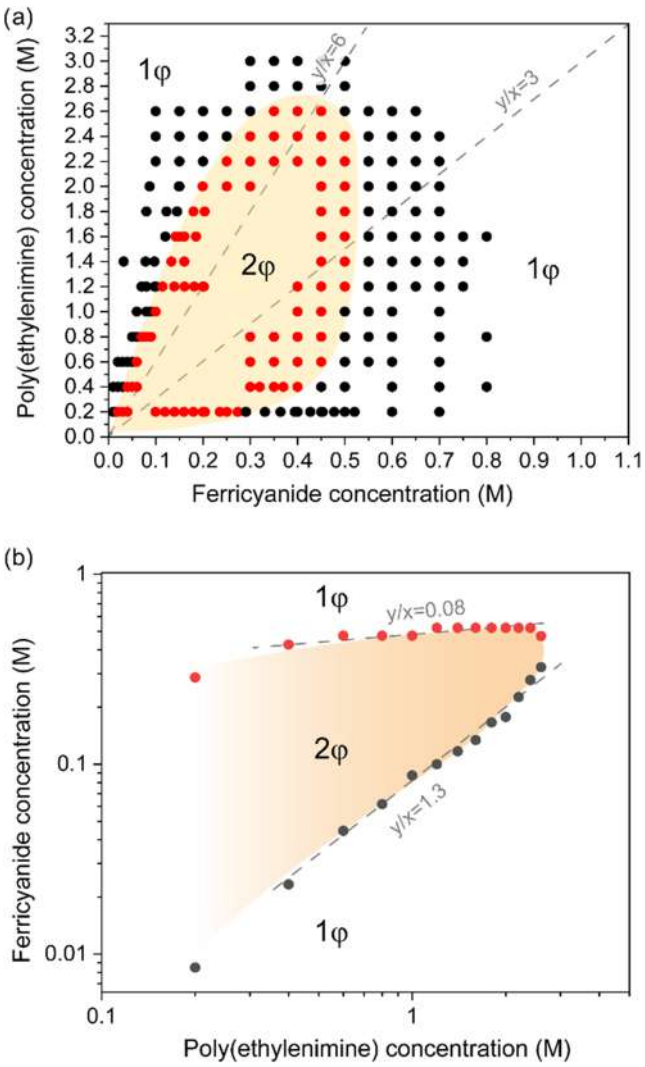

Figure 2. (a) Phase diagram in the [PEI] *vs* [$Fe(CN)_6^{3-}$] plane in a linear scale. Red dots inside the two-phase region (2φ) indicate solutions in which LLPS occurs. Black dots outside the one-phase region (area labeled as 1φ) indicate solutions in which LLPS does not occur. (b) [$Fe(CN)_6^{3-}$] *vs* [PEI] plot in a logarithmic scale (black and red dots correspond to the left and right contour branches of the upper diagram).

if one could plot the full 5D phase diagram of the system, the composition of the minority phase would lie in a plane different to that plotted in Figure 2a). Finally, since the phase diagram is a 2D cut of the full multidimensional diagram of the system and the binodal line indicates only the composition of the majority phase, tie lines cannot be represented in this plot. A strict thermodynamically analysis is even more complex than the one discussed above because the protonation state of the amino groups may be affected by their interaction with $Fe(CN)_6^{3-}$.[57] In the next section, we describe the results of our approximate thermodynamic model, which takes into consideration the previous observations and it is able to fit the experimental data.

The two-phase region in the [$Fe(CN)_6^{3-}$] *vs* [PEI] plane in Figure 2a has a deformed elliptical shape, similar to the phase diagram obtained using the Voorn−Overbeek theory for a system composed of two polyelectrolytes.[4] This observation supports our hypothesis that the polycation/multivalent-ion

https://doi.org/10.1021/acs.jpcb.3c03680
J. Phys. Chem. B 2023, 127, 7636−7647

system is just a particular case of polycation/polyanion coacervate. In other words, the PEI/$Fe(CN)_6^{3-}$ coacervate can be simply treated as a highly asymmetric case of polycation/polyanion coacervates, where the polyanion has a very short length. On the other hand, there are quantitative differences between the phase diagrams of the polycation/multivalent-ion and the polycation/polyanion systems. Symmetric coacervates have a symmetric phase diagram, where the principal axis of the "ellipse" mentioned above coincides with the line with slope [polycation]/[polyanion] = 1 (where the concentrations of polymeric species are always given in terms of monomers).[4] However, unlike the fully symmetric polycation/polyanion case, the principal axis of the "ellipsoid" in the phase diagram of Figure 2a coincides with the line with a slope [PEI]/[$Fe(CN)_6^{3-}$] = 6. Assuming that all monomers in PEI can interact with $Fe(CN)_6^{3-}$ would result in a slope of [PEI]/[$Fe(CN)_6^{3-}$] = 3. On the other hand, taking into consideration the experimentally measured protonation fraction of 0.3 for PEI[56] and assuming the state of protonation does not substantially change upon complexation, resulting in an expected stoichiometric ratio of [PEI]/[$Fe(CN)_6^{3-}$] = 10, which is now higher than that in Figure 2a. Therefore, one possible explanation for the results in Figure 2a is that upon interaction with $Fe(CN)_6^{3-}$, the fraction of protonated PEI monomers increases to 0.5 (which would yield the observed slope of [PEI]/[$Fe(CN)_6^{3-}$] = 6). However, our theoretical predictions (discussed below) provide an alternative explanation: the phase diagram of the polycation/multivalent-ion has an intrinsic asymmetry, even when plotted in terms of the real charge concentration, which results from the strong difference in the number of charges per molecule of the two involved macroions.

Another interesting conclusion that can be extracted from the phase diagram in Figure 2a is that a plot of the binodal curve in a log−log scale reproduces the universal curve typically observed for polyelectrolyte/multivalent-ion phase diagrams (Figure 2b). Similar curves were observed by many authors for DNA/spermine[20,58] and for the combination of different polyanions with multivalent cations.[59,60] The fact that the PEI/$Fe(CN)_6^{3-}$ system reproduces well both the polycation/polyanion (Figure 2a) and polyelectrolyte/multivalent-ion (Figure 2b) phase diagrams seems to indicate that these (apparently) different systems are governed by the same physical−chemical mechanisms. This is a nontrivial conclusion because the reentrant behavior of these two systems was explained in the literature by using different arguments.[33,61]

A key feature of polyelectrolyte complexes is their tendency to dissolve (*i.e.*, to dissociate) at elevated ionic strengths. For a typical polyelectrolyte/multivalent-ion system, it was demonstrated that the two-phase region in the phase diagram (Figure 2a,b) narrows until completely disappearing upon increasing the concentration of an added monovalent salt.[59] A similar phenomenon was reported for polycation/polyanion complexes.[22] The minimum concentration of monovalent ions necessary to produce the dissolution of the complex is called the salt resistance. The salt resistance in polyelectrolyte complexes varies with the concentration of complexing species in a non-monotonic way;[2,3,22,23,30,31] therefore, it is common to study it as a function of the total concentration of the polymers. In this case, as the system is composed of a polycation and a multivalent ion, we measured and plotted in Figure 3 the salt resistance for different PEI concentrations at fixed [PEI]/[$Fe(CN)_6^{3-}$] = 6 (this ratio maximizes the range

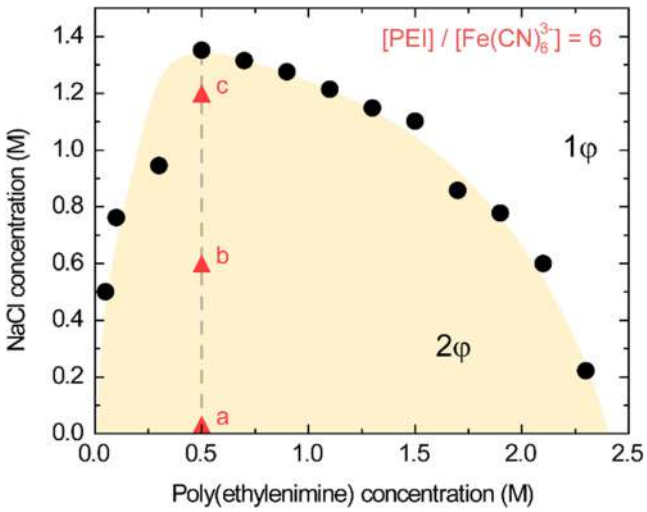

Figure 3. Phase diagram in the plane of added [NaCl] *vs* [PEI] (for fixed [PEI]/[$Fe(CN)_6^{3-}$] = 6). The points a, b, and c were used to study the electrochemical response of the system. 2φ (two-phase) and 1φ (one-phase) regions correspond to areas where LLPS does and does not occur.

of concentrations where LLPS occurs; see Figure 2a and the discussion above). Note that the plot in Figure 3 is also a 2D cut (different from that shown in Figure 2a) of the full multidimensional phase diagram; therefore, tie lines cannot be represented in this plot. It is also interesting to realize that each different [PEI]/[$Fe(CN)_6^{3-}$] slope in the phase diagram of Figure 2a will lead to a different salt-resistance plot (*i.e.*, a different plane in the multidimensional phase diagram).

The salt resistance in Figure 3 displays a maximum at [PEI] = 0.5 M and [NaCl] = 1.35 M (known as the critical salt concentration). When exceeding 2.5−2.7 M of PEI, the system does not phase-separate even at zero added monovalent salt. The shape of the salt-resistance plot in Figure 3 is similar to the typical binodal phase diagram of symmetric polyelectrolyte complexes in the [salt] *vs* [total polyelectrolyte] plane.[62] This observation agrees well with the idea of considering PEI/$Fe(CN)_6^{3-}$ as an asymmetric polyelectrolyte complex.

3.2. Theoretical Model of Asymmetric Coacervates.

As discussed in the previous paragraphs, our experimental evidence suggests that the PEI/$Fe(CN)_6^{3-}$ system is just a highly asymmetric case of the well-known polycation/polyanion coacervates. From this point of view, it is natural to attempt modeling it with the same tools developed for polyelectrolyte coacervates. Such analysis may shed light on how the strong asymmetry of the system is manifested in its phase behavior. In previous publications,[23,45] we developed a model for (symmetric) polyelectrolyte coacervates based on a chemical-equilibrium formalism.[30,43] In this formalism, the formation of ion pairs between the polycation and the polyanion and between the polyelectrolytes and the small salt ions is described using chemical-equilibria equations. This approach can quantitatively fit phase diagrams in the literature,[23] although at the cost of introducing a few fitting (although still chemically meaningful) parameters: the chemical-equilibrium constants, which are absent in other models for polyelectrolyte coacervation.[25−28,33,63] In this work, we extended the chemical-equilibrium formalism to polyanion/polycation pairs, where the two components are asymmetric both in terms of their charge and concentration.

https://doi.org/10.1021/acs.jpcb.3c03680
J. Phys. Chem. B 2023, 127, 7636−7647

The construction of the binodal phase diagram requires finding two phases with different compositions that have the same chemical potentials for all species and the same thermodynamic pressure. In our model, expressions for the chemical potentials and the thermodynamic pressure are obtained through the proper derivatives of an approximate free-energy functional of the system (see Theoretical Methods and the Supporting Information). The resulting expressions constitute a set of nonlinear coupled equations that cannot be analytically solved. In order to fit the experimental phase diagram shown in Figure 2a, we fixed the concentration of added salt in one of the phases (the majority phase, whose composition is reported in the phase diagram; see the discussion above). Then, we scanned the concentration of one of the macroions in that phase (*e.g.*, PEI). For each concentration of the macroion, we attempted to numerically solve the set of coupled equations mentioned above. If successful, this procedure yields the composition of the coexisting phase, the difference of electrostatic potentials between both phases (Donnan potential difference), and the difference of osmotic pressures between both phases, as well as the concentration of the other macroion in the phase reported in the diagram (thereby, allowing us to place a point in the diagram). Failure to converge the set of analytical equations indicates that phase coexistence cannot occur for the concentration chosen as the independent variable. This procedure is described in further detail in the Supporting Information. On the other hand, a comprehensive analysis of the theoretical predictions of our model regarding the composition of the coexisting minority phase, the difference of electrostatic potentials, and osmotic pressures between both phases is outside the scope of this work and will be reported elsewhere.

The phase diagram predicted by our model depends on the following input parameters: (i) the number of charges per macroanion (fixed to 3 in the case of $Fe(CN)_6^{3-}$) and of the polycation, (ii) the values of the equilibrium constants for the macroion/macroion and ion/macroion ion-pairing reactions (*i.e.*, the equilibrium constants associated with eqs 3−5), and (iii) the concentration of the added monovalent salt (which is fixed to its experimental value). We fixed the number of charges per PEI molecule to 170, as estimated from its degree of polymerization (n = 570) and its fraction of protonation (f = 0.3[56]). The equilibrium constants were treated as fitting parameters. Figure 4a,b shows that our model can simultaneously fit all of the experimental data available for the PEI/$Fe(CN)_6^{3-}$ system. The best fitting parameters were K_{as} = 0.12 [M^{-1}] (equilibrium constant for macroion−macroion association, process shown in eq 3) and $K_{as\text{-}ion}$ = 1.23 [M^{-1}] (equilibrium constants for macroion−monovalent ion association, eqs 4 and 5). These two parameters are of the same order of magnitude as those obtained by fitting polycation/polyanion coacervates in our previous work,[43] which strengthens our conclusion that PEI/$Fe(CN)_6^{3-}$ can be described as a particular (highly asymmetric) case of the most general polyanion/polycation case. Note that in Figure 4a, we plotted the diagram using charge concentrations (instead of monomer concentrations for PEI) in order to emphasize the deviation from the 1:1 charge stoichiometry.

It is worthwhile to stress that the equilibrium constants obtained by fitting the experimental phase diagrams represent the binding of a single association site (*i.e.*, a charged site) of the macroion with an oppositely charged monovalent ion in solution ($K_{as\text{-}ion}$, eqs 4 and 5) or a single association site in the other macroion (K_{as}). Correlations between the state of binding of neighbor sites are neglected, and, therefore, the association constants are independent of the state of binding of the other sites in the macroion, and they should be regarded as average values over all possible configurations of the system. Finally, note that we used the same association constant, $K_{as\text{-}ion}$, for the ferricyanide-cation and PEI-anion ion pairs. As we discuss in detail in the Supporting Information, there are several combinations of association constants for these two reactions that result in the same predicted phase diagram; therefore (in the absence of additional experimental evidence),

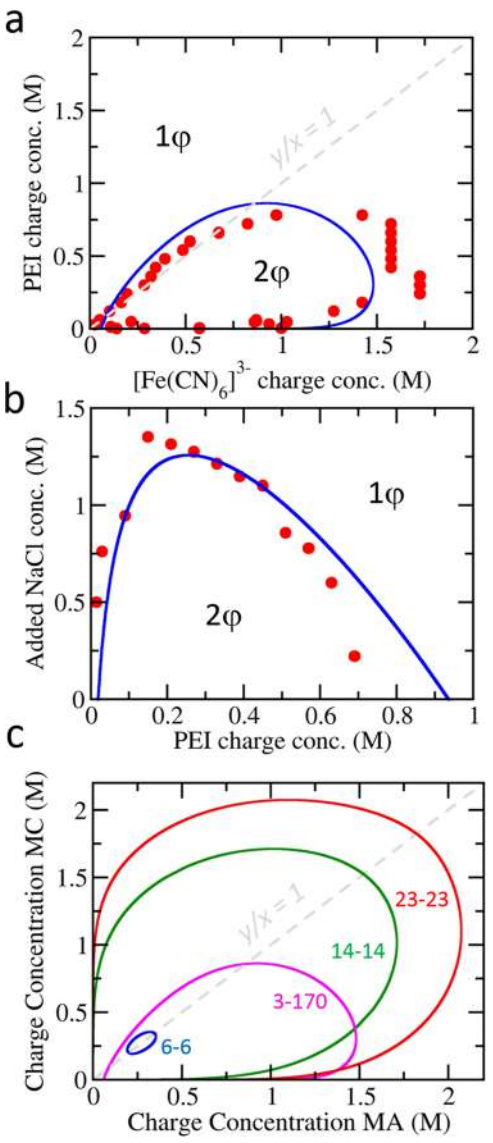

Figure 4. (a, b) Comparison between experimental (red symbols) and theoretically predicted (blue line) phase diagram for the PEI/$Fe(CN)_6^{3-}$ system in the planes given by (a) charge concentration of the macroions for fixed 0.5 M added NaCl and (b) concentration of added NaCl *vs* the charge concentration of PEI for a fixed PEI/$Fe(CN)_6^{3-}$ molar ratio of 6. 2φ and 1φ regions correspond to areas where LLPS does and does not occur. (c) Theoretically predicted phase diagrams in the same conditions of panel (a) but for macroion pairs of different changes per molecule, where the labels indicate the charge of the macroanion and the macrocation, *e.g.*, 3−170 indicates a macroanion of 3 charges and a macrocation of 170 charges.

https://doi.org/10.1021/acs.jpcb.3c03680
J. Phys. Chem. B 2023, 127, 7636−7647

we decided to use the same value for both reactions to reduce the number of fitting parameters.

In Figure 4c, we use the fitting parameters obtained from Figure 4a,b to gain a better understanding of the phase diagrams. The "170-3" curve in Figure 4c indicates a macrocation with 170 charges/molecules and a macroanion with 3 charges/molecule, *i.e.*, the PEI/$Fe(CN)_6^{3-}$ case. As shown above, this curve is highly asymmetric with respect to the charge-stoichiometry line (y/x = 1). On the contrary, charge-symmetric systems (23−23, 14−14, and 6−6) produce symmetric phase diagrams. Note that there is a very strong stabilization of the two-phase region when increasing the number of charges per macroion. Finally, for a fixed value of equilibrium constants, the two-phase region of the 170−3 case is much smaller than that of the 23−23, which indicates that coacervates from small multivalent ions and polyelectrolytes are expected to be less stable than coacervates formed by two polyelectrolytes (provided that the interactions in both cases and the molecular weight of the polyelectrolytes are similar).

The predictions of our model can be rationalized by considering the balance of the ion-pairing free energy gained upon complexation and the penalty in translation entropy resulting from creating two liquid phases of different compositions. For a given number of charges involved in complexation, the relative importance of this entropic penalty decreases when increasing the number of charges per molecule. Therefore, increasing the charges per macroion stabilizes the formation of the coacervate. This argument also explains why in the case of asymmetric coacervates, most of the binodal region in Figure 4a,c is below the 1:1 charge-stoichiometry line. PEI/$Fe(CN)_6^{3-}$ coacervates are most stable when the total number of charges from PEI in the system is smaller than those from $Fe(CN)_6^{3-}$. When the initial composition of the system is nonstoichiometric, most of the translational entropic penalty upon the formation of the coacervate results from the partition of macroion in stoichiometric defect (*i.e.*, the "limiting reagent" for the formation of the coacervate) because that species will be the one showing the highest difference of composition between the dilute and the coacervate phases. Therefore, in the case when the limiting species is PEI (which has ∼170 charges per molecule and thus produces only a small entropic penalty), the formation of the coacervate is more stable than in the case when the limiting species is $Fe(CN)_6^{3-}$ (which has 3 charges per molecule and thus produces a large entropic penalty).

3.3. Charge Transport in PEI/$Fe(CN)_6^{3-}$ Coacervates.

We now shift our attention to the electrochemical response of the PEI/$Fe(CN)_6^{3-}$ system. Figure 5a shows the cyclic voltammograms measured for the PEI/$Fe(CN)_6^{3-}$ coacervate phase for two different concentrations of added NaCl. In both cases, well-defined oxidation and reduction peaks are observed. The peak separation ΔE_p in both voltammograms is larger than the ideal value of 59.6 mV for a single-electron redox couple in solution and an electrochemical reversible process (*i.e.*, a process where electron transfer at the electrode is much faster than the measurement timescale).[64−66] The fact that the peak separation, ΔE_p, is larger than 59.6 mV indicates either a large ohmic drop (due to poor solution conductivity) or a quasi-reversible electrochemical response (due to sluggish heterogeneous electron transfer at the solution−electrode interface). To discern which of these two mechanisms is dominant, we plotted ΔE_p as a function of the square root of the scan rate ($v^{1/2}$) (Figure 5b). A linear relationship was obtained in all

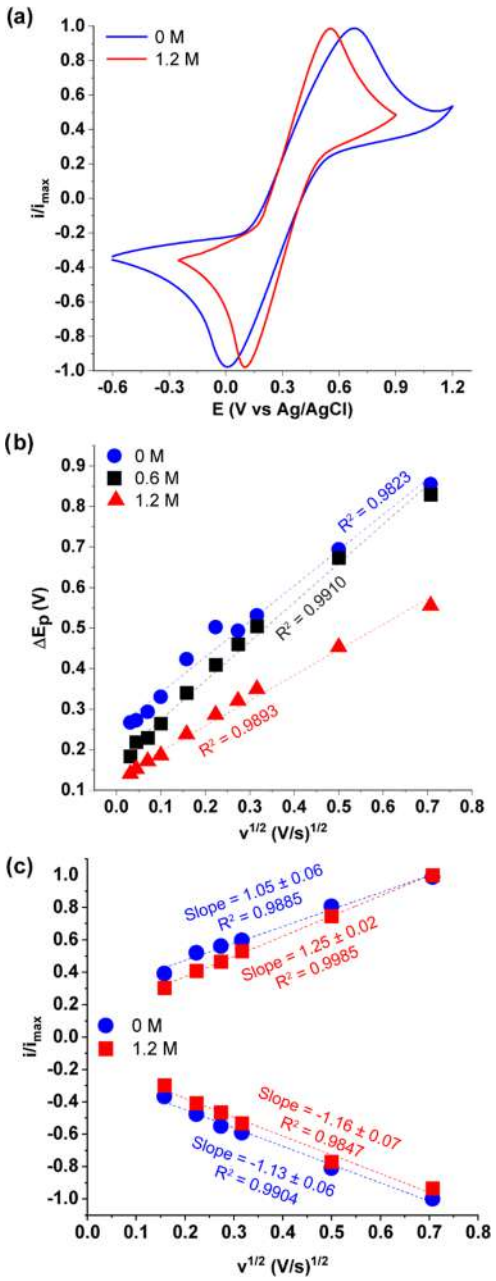

Figure 5. (a) Cyclic voltammograms recorded at 250 mV/s for PEI/$Fe(CN)_6^{3-}$ coacervates formed in the presence of NaCl 0 or 1.2 M. (b) Separation of the anodic and cathodic peak potentials *versus* the square root of scan rate, $v^{1/2}$, measured for coacervates prepared with different concentrations of added NaCl. (c) Peak currents for the anodic ($i/i_{max} > 0$) and cathodic ($i/i_{max} < 0$) *vs* $v^{1/2}$ measured for coacervates formed in the presence of NaCl 0 M or 1.2 M *versus* the scan rate. The currents are normalized by i_{max}, which is the peak current determined for $v^{1/2}$ = 0.707 $(V/s)^{1/2}$ (0.5 V/s).

cases, which indicates that uncompensated resistance is small and that the system has a slow heterogeneous electron transfer at the electrode/solution interface.[67,68] In summary, the electrochemical response of the redox coacervate is controlled by both diffusional mass transport in solution and charge-transfer kinetics at the electrode/solution interface and, therefore, PEI/$Fe(CN)_6^{3-}$ coacervates are *quasi*-reversible electrochemical systems[64−66] (this conclusion is further supported by a detailed analysis of the effect of the scan rate

https://doi.org/10.1021/acs.jpcb.3c03680
J. Phys. Chem. B 2023, 127, 7636−7647

on peak potential and current; see the discussion in the Supporting Information).

It is interesting to note that the electrochemical reversibility in Figure 5a improves (*i.e.*, the peak separation decreases) upon the addition of NaCl. This result is expected because the added salt partially breaks some ionic bonds between macroions in the coacervate, thus decreasing its viscosity[49,69,70] and increasing the mobility of the macroions. An improved translational and rotational mobility of $Fe(CN)_6^{3-}$ near the electrode can thus lead to improved heterogeneous charge transport. We provide below a quantification of the effect of added salt on the properties of the system.

As discussed above, the electrochemical behavior of PEI/$Fe(CN)_6^{3-}$ is determined by both diffusional mass transport (controlled by the apparent diffusion coefficient for charge transport, D) and the charge-transfer kinetics at the electrode (controlled by the heterogeneous rate constant, k^0). The diffusion coefficient for charge transport when $\Delta E_p > 200$ mV can be obtained from the slope of a plot of i_p (peak current) with $v^{1/2}$ (v is the scan rate), according to the equation[64,67]

$$i_p = 2.99 \times 10^5 n^{3/2} \alpha^{1/2} A C D^{1/2} v^{1/2} \quad (8)$$

where α is the charge-transfer coefficient, A is the electrode geometric area, and C is the concentration of $Fe(CN)_6^{3-}$ in the coacervate (which we determined using UV–vis). Figure 5c shows the i_p *vs* $v^{1/2}$ plots and Table 1 compiles the values of D

Table 1. Salt Concentration Used to Form the Coacervate, $[NaCl]_{added}$, Concentration of Ferricyanide in the Coacervate, C, Diffusion Coefficients Measured by CV and EIS (D), and Standard Rate Constant Measured by CV (k^0)

$[NaCl]_{added}$ (M)	C (M)	D ($cm^2\ s^{-1}$) (CV)	k^0 ($cm\ s^{-1}$) (CV)	D ($cm^2\ s^{-1}$) (EIS)
0	0.416	2.2×10^{-8}	2.4×10^{-4}	1.3×10^{-8}
0.6	0.353	9.7×10^{-8}	4.7×10^{-4}	3.3×10^{-8}
1.2	0.286	2.2×10^{-7}	5.4×10^{-4}	5.6×10^{-8}

obtained from the linear fit. In the absence of NaCl, the diffusion coefficient is around two orders of magnitude lower than the respective value reported for ferricyanide in aqueous solution at room temperature (7.3×10^{-6} $cm^2\ s^{-1}$).[71] Interestingly, when the coacervate is formed in the presence of 0.6 and 1.2 M NaCl, D increases by factors of 4.5 and 9.4, respectively. We also included in Table 1 a set of values determined using electrochemical impedance spectroscopy (EIS) on the same samples (see the Supporting Information), which are systematically smaller by a factor between 1.5 and 4 than those determined by CV, but display the same trend with added salt concentration, thereby supporting our conclusions.

We also characterized the heterogeneous standard rate constant for electron transfer at the solution/electrode interface (k^0) using the following relationship[64,72]

$$i_p = 2.27 \times 10^{-4} nFCk^0 \exp(\alpha F(E_p - E^0)/RT) \quad (9)$$

where E_p is the peak potential, E^0 is the apparent redox potential of the couple and the other parameters were defined above. Figure S2 shows that plotting $\ln(i_p)$ *vs* $(E_p - E^0)$ for our data produces linear plots (as predicted by eq 9). We obtained the values of k^0 from the slopes of these plots and compiled them in Table 1. All k^0 values are close to 10^{-4} $cm^2\ s^{-1}$, which is the range expected for a quasi-reversible system (10^{-1} to 10^{-5} cm s^{-1})[64,72] and are similar to those obtained for ferricyanide in KF solutions up to 1 M.[72] The values of k^0 slightly but monotonically increase with increasing salt concentration.

It is important to realize that the three coacervates reported in Table 1 contain different concentrations of PEI and $Fe(CN)_6^{3-}$ because the concentration of salt influences the phase diagram of the system (see Figure 3). Therefore, it is important to determine whether the increase in D by added NaCl is originated in the salt concentration of the coacervate or, instead, is an indirect consequence of the different concentrations of PEI and $Fe(CN)_6^{3-}$. To address this question, we added solid NaCl salt to a coacervate initially prepared in the absence of added NaCl in order to obtain final NaCl concentrations of 0.6 or 1.2 M. Therefore, these three samples have the same concentrations of PEI and $Fe(CN)_6^{3-}$, but different concentrations of NaCl. The values of D determined for these samples were 2.20×10^{-8}, 1.14×10^{-7}, and 1.16×10^{-7} cm^2/s for added NaCl concentrations of 0, 0.6, and 1.2 M, respectively. This result supports the hypothesis that the addition of monovalent salt directly affects the value of D by breaking macroion–macroion ion pairs.

4. CONCLUSIONS

In this work, we reported the preparation of liquid coacervates of PEI and $Fe(CN)_6^{3-}$, systematically characterized their phase behavior, and explored their electrochemical properties. Interestingly, polyelectrolyte coacervates and polyelectrolyte/multivalent-ion complexes are two systems that are currently attracting great interest, but had evolved as two independent, scarcely connected fields. We believe that this situation can be (at least partially) attributed to the fact that our experimental and theoretical understanding of the phase behavior of polyelectrolyte coacervates derives mainly from studies of symmetric polyelectrolyte pairs. Moreover, most studies addressing polyelectrolyte/multivalent-ion complexes (polyamine/salt,[19] spermine/DNA,[20] polyanion/divalent ions,[60] etc.) only studied and characterized narrow regions of the corresponding full phase diagrams (*i.e.*, limited ranges of concentration). We argue that polyelectrolyte/multivalent-ion complexes can be regarded as a specific (highly asymmetrical) type of the polyelectrolyte/polyelectrolyte complex and, therefore, they can be effectively approached and analyzed within the framework of polyanion/polycation complexes. The following observations for the PEI and $Fe(CN)_6^{3-}$ support this hypothesis: (i) like polyanion/polycation complexes, polyamine/$Fe(CN)_6^{3-}$ can produce both solid complexes and liquid coacervates, (ii) the phase diagrams of the PEI/$Fe(CN)_6^{3-}$ system (Figures 2a and 3) have the same qualitative behavior as those of polyanion/polycation systems, and (iii) we were able to model the aforementioned diagrams using the same theoretical formalism previously used to model polyelectrolyte/polyelectrolyte coacervates[23] and obtained chemical association constants of a similar order of magnitude for both cases. We believe that these observations provide critical support to our claim that polyelectrolyte/multivalent-ion complexes are a specific subclass of polyelectrolyte/polyelectrolyte complexes.

In the second part of this work, we provided the first exploration of the electrochemical behavior of a redox coacervate. The two most important conclusions of this study are (i) the electrochemical activity of $Fe(CN)_6^{3-}$ is maintained within the coacervate and this redox couple displays a quasi-reversible electrochemical behavior, and (ii)

https://doi.org/10.1021/acs.jpcb.3c03680
J. Phys. Chem. B 2023, 127, 7636–7647

addition of a monovalent salt to the system improves the electrochemical reversibility (*i.e.*, it increases the charge-transport diffusion coefficient and the heterogeneous electron-transfer rate constant). We attribute this behavior to the well-known doping of polyanion/polycation intrinsic ion pairs by added salt,[49,73] which in our case should increase the mobility of $Fe(CN)_6^{3-}$ within the coacervate. Future work will be aimed to explore in additional detail the mechanisms of diffusional charge transport of $Fe(CN)_6^{3-}$ and to establish relationships between its electrochemical response and rheological properties, as well as to explore potential applications for this new class of highly asymmetrical electroactive coacervate.

■ ASSOCIATED CONTENT

Supporting Information

The Supporting Information is available free of charge at https://pubs.acs.org/doi/10.1021/acs.jpcb.3c03680.

Detailed analysis of the electrochemical response of PEI/$Fe(CN)_6^{3-}$ coacervates; electrochemical impedance spectroscopy (EIS) of PEI/$Fe(CN)_6^{3-}$ coacervates; $\ln(i_p)$ *vs* $E_p - E_0$ plots used to determine the values of heterogeneous rate constants; and detailed description of the theoretical method to calculate the binodal phase diagrams and effect of macrocation−anion and macroanion−cation association constants (PDF)

■ AUTHOR INFORMATION

Corresponding Authors

Santiago E. Herrera − *Facultad de Ciencias Exactas y Naturales, Departamento de Química Inorgánica Analítica y Química Física, Universidad de Buenos Aires, C1428 Ciudad Autónoma de Buenos Aires, Argentina; Facultad de Ciencias Exactas y Naturales, Instituto de Química de los Materiales, Ambiente y Energía (INQUIMAE), CONICET—Universidad de Buenos Aires, C1428 Ciudad Autónoma de Buenos Aires, Argentina;* orcid.org/0000-0002-8327-3914; Email: sherrera@qi.fcen.uba.ar

Mario Tagliazucchi − *Facultad de Ciencias Exactas y Naturales, Departamento de Química Inorgánica Analítica y Química Física, Universidad de Buenos Aires, C1428 Ciudad Autónoma de Buenos Aires, Argentina; Facultad de Ciencias Exactas y Naturales, Instituto de Química de los Materiales, Ambiente y Energía (INQUIMAE), CONICET—Universidad de Buenos Aires, C1428 Ciudad Autónoma de Buenos Aires, Argentina;* orcid.org/0000-0003-4755-955X; Email: mario@qi.fcen.uba.ar

Authors

Lucy L. Coria-Oriundo − *Facultad de Ciencias Exactas y Naturales, Departamento de Química Inorgánica Analítica y Química Física, Universidad de Buenos Aires, C1428 Ciudad Autónoma de Buenos Aires, Argentina; Facultad de Ciencias Exactas y Naturales, Instituto de Química de los Materiales, Ambiente y Energía (INQUIMAE), CONICET—Universidad de Buenos Aires, C1428 Ciudad Autónoma de Buenos Aires, Argentina;* orcid.org/0000-0003-3502-4726

Gabriel Debais − *Facultad de Ciencias Exactas y Naturales, Departamento de Química Inorgánica Analítica y Química Física, Universidad de Buenos Aires, C1428 Ciudad Autónoma de Buenos Aires, Argentina; Facultad de Ciencias Exactas y Naturales, Instituto de Química de los Materiales, Ambiente y Energía (INQUIMAE), CONICET—Universidad de Buenos Aires, C1428 Ciudad Autónoma de Buenos Aires, Argentina*

Eugenia Apuzzo − *Instituto de Investigaciones Fisicoquímicas Teóricas y Aplicadas (INIFTA-CONICET), Departamento de Química, Facultad de Ciencias Exactas, Universidad Nacional de La Plata, 1900 La Plata, Argentina*

Marcelo Ceolín − *Instituto de Investigaciones Fisicoquímicas Teóricas y Aplicadas (INIFTA-CONICET), Departamento de Química, Facultad de Ciencias Exactas, Universidad Nacional de La Plata, 1900 La Plata, Argentina*

Omar Azzaroni − *Instituto de Investigaciones Fisicoquímicas Teóricas y Aplicadas (INIFTA-CONICET), Departamento de Química, Facultad de Ciencias Exactas, Universidad Nacional de La Plata, 1900 La Plata, Argentina;* orcid.org/0000-0002-5098-0612

Fernando Battaglini − *Facultad de Ciencias Exactas y Naturales, Departamento de Química Inorgánica Analítica y Química Física, Universidad de Buenos Aires, C1428 Ciudad Autónoma de Buenos Aires, Argentina; Facultad de Ciencias Exactas y Naturales, Instituto de Química de los Materiales, Ambiente y Energía (INQUIMAE), CONICET—Universidad de Buenos Aires, C1428 Ciudad Autónoma de Buenos Aires, Argentina;* orcid.org/0000-0002-1113-1642

Complete contact information is available at: https://pubs.acs.org/10.1021/acs.jpcb.3c03680

Author Contributions

The manuscript was written through contributions of all authors. All authors have given approval to the final version of the manuscript.

Notes

The authors declare no competing financial interest.

■ ACKNOWLEDGMENTS

S.E.H., M.C., O.A., F.B., and M.T. are fellows of CONICET. The authors acknowledge financial support from (ANPCyT) PICT 1520-2019 and PICT 00492-2021 and from CONICET PIP 71511220200102008CO.

■ REFERENCES

(1) Srivastava, S.; Tirrell, M. V.Polyelectrolyte Complexation. In *Advances in Chemical Physics*; John Wiley & Sons, 2016; Vol. *161*, pp 499−544.

(2) Rumyantsev, A. M.; Jackson, N. E.; de Pablo, J. J. Polyelectrolyte Complex Coacervates: Recent Developments and New Frontiers. *Annu. Rev. Condens. Matter Phys.* **2021**, *12*, 155−176.

(3) Sing, C. E. Development of the Modern Theory of Polymeric Complex Coacervation. *Adv. Colloid Interface Sci.* **2017**, *239*, 2−16.

(4) van der Gucht, J.; Spruijt, E.; Lemmers, M.; Stuart, M. A. C. Polyelectrolyte Complexes: Bulk Phases and Colloidal Systems. *J. Colloid Interface Sci.* **2011**, *361*, 407−422.

(5) Sing, C. E.; Perry, S. L. Recent Progress in the Science of Complex Coacervation. *Soft Matter* **2020**, *16*, 2885−2914.

(6) Moulik, S. P.; Rakshit, A. K.; Pan, A.; Naskar, B. An Overview of Coacervates: The Special Disperse State of Amphiphilic and Polymeric Materials in Solution. *Colloids Interfaces* **2022**, *6*, No. 45.

(7) Michaels, A. S. Polyelectrolyte complexes. *Ind. Eng. Chem.* **1965**, *57*, 32−40.

(8) Herrera, S. E.; Agazzi, M. L.; Apuzzo, E.; Cortez, M. L.; Marmisollé, W. A.; Tagliazucchi, M.; Azzaroni, O. Polyelectrolyte-

Multivalent Molecule Complexes: Physicochemical Properties and Applications. *Soft Matter* **2023**, *19*, 2013−2041.
(9) Jong, H. G. B.; Kruyt, H. R. Koazervation: Entmischung in kolloiden Systemen. *Kolloid-Z.* **1930**, *50*, 39−48.
(10) de Jong, H. G. B.; Kruyt, H. Coacervation (Partial Miscibility in Colloid Systems). *Proc. K. Ned. Akad. Wet.* **1929**, *32*, 849−856.
(11) Abbas, M.; Lipiński, W. P.; Wang, J.; Spruijt, E. Peptide-Based Coacervates as Biomimetic Protocells. *Chem. Soc. Rev.* **2021**, *50*, 3690−3705.
(12) Jho, Y.; Yoo, H. Y.; Lin, Y.; Han, S.; Hwang, D. S. Molecular and Structural Basis of Low Interfacial Energy of Complex Coacervates in Water. *Adv. Colloid Interface Sci.* **2017**, *239*, 61−73.
(13) Meng, S.; Ting, J. M.; Wu, H.; Tirrell, M. V. Solid-to-Liquid Phase Transition in Polyelectrolyte Complexes. *Macromolecules* **2020**, *53*, 7944−7953.
(14) Priftis, D.; Megley, K.; Laugel, N.; Tirrell, M. Complex Coacervation of Poly(Ethylene-Imine)/Polypeptide Aqueous Solutions: Thermodynamic and Rheological Characterization. *J. Colloid Interface Sci.* **2013**, *398*, 39−50.
(15) Liu, X.; Xu, J.; Xie, X.; Ma, Z.; Zheng, T.; Wu, L.; Li, B.; Li, W. Heteropoly Acid-Driven Assembly of Glutathione into Redox-Responsive Underwater Adhesive. *Chem. Commun.* **2020**, *56*, 11034−11037.
(16) Shao, H.; Bachus, K. N.; Stewart, R. J. A Water-Borne Adhesive Modeled after the Sandcastle Glue of *P. californica*: A Water-Borne Adhesive Modeled after the Sandcastle Glue of *P. californica*. *Macromol. Biosci.* **2009**, *9*, 464−471.
(17) McTigue, W. C. B.; Perry, S. L. Design Rules for Encapsulating Proteins into Complex Coacervates. *Soft Matter* **2019**, *15*, 3089−3103.
(18) Lapitsky, Y. Ionically Crosslinked Polyelectrolyte Nanocarriers: Recent Advances and Open Problems. *Curr. Opin. Colloid Interface Sci.* **2014**, *19*, 122−130.
(19) Herrera, S. E.; Agazzi, M. L.; Cortez, M. L.; Marmisollé, W. A.; Tagliazucchi, M.; Azzaroni, O. Polyamine Colloids Cross-Linked with Phosphate Ions: Towards Understanding the Solution Phase Behavior. *ChemPhysChem* **2019**, *20*, 1044−1053.
(20) Hoopes, B. C.; McClure, W. R. Studies on the Selectivity of DNA Precipitation by Spermine. *Nucleic Acids Res.* **1981**, *9*, 5493−5504.
(21) Li, L.; Srivastava, S.; Andreev, M.; Marciel, A. B.; de Pablo, J. J.; Tirrell, M. V. Phase Behavior and Salt Partitioning in Polyelectrolyte Complex Coacervates. *Macromolecules* **2018**, *51*, 2988−2995.
(22) Spruijt, E.; Westphal, A. H.; Borst, J. W.; Stuart, M. A. C.; van der Gucht, J. Binodal Compositions of Polyelectrolyte Complexes. *Macromolecules* **2010**, *43*, 6476−6484.
(23) Debais, G.; Tagliazucchi, M. The Two Sides of the Same Coin: A Unified Theoretical Treatment of Polyelectrolyte Complexation in Solution and Layer-by-Layer Films. *Macromolecules* **2022**, *55*, 5263−5275.
(24) Kudlay, A.; Ermoshkin, A. V.; de La Cruz, M. O. Complexation of Oppositely Charged Polyelectrolytes: Effect of Ion Pair Formation. *Macromolecules* **2004**, *37*, 9231−9241.
(25) Castelnovo, M.; Joanny, J.-F. Complexation between Oppositely Charged Polyelectrolytes: Beyond the Random Phase Approximation. *Eur. Phys. J. E* **2001**, *6*, 377−386.
(26) Ermoshkin, A. V.; de La Cruz, M. O. A Modified Random Phase Approximation of Polyelectrolyte Solutions. *Macromolecules* **2003**, *36*, 7824−7832.
(27) Castelnovo, M.; Joanny, J. F. Formation of Polyelectrolyte Multilayers. *Langmuir* **2000**, *16*, 7524−7532.
(28) Delaney, K. T.; Fredrickson, G. H. Theory of Polyelectrolyte Complexation—Complex Coacervates Are Self-Coacervates. *J. Chem. Phys.* **2017**, *146*, No. 224902.
(29) Lee, J.; Popov, Y. O.; Fredrickson, G. H. Complex Coacervation: A Field Theoretic Simulation Study of Polyelectrolyte Complexation. *J. Chem. Phys.* **2008**, *128*, No. 224908.
(30) Salehi, A.; Larson, R. G. A Molecular Thermodynamic Model of Complexation in Mixtures of Oppositely Charged Polyelectrolytes with Explicit Account of Charge Association/Dissociation. *Macromolecules* **2016**, *49*, 9706−9719.
(31) Salehi, A.; Desai, P. S.; Li, J.; Steele, C. A.; Larson, R. G. Relationship between Polyelectrolyte Bulk Complexation and Kinetics of Their Layer-by-Layer Assembly. *Macromolecules* **2015**, *48*, 400−409.
(32) Chen, S.; Zhang, P.; Wang, Z.-G. Complexation between Oppositely Charged Polyelectrolytes in Dilute Solution: Effects of Charge Asymmetry. *Macromolecules* **2022**, *55*, 3898−3909.
(33) Zhang, P.; Alsaifi, N. M.; Wu, J.; Wang, Z.-G. Polyelectrolyte Complex Coacervation: Effects of Concentration Asymmetry. *J. Chem. Phys.* **2018**, *149*, No. 163303.
(34) Friedowitz, S.; Salehi, A.; Larson, R. G.; Qin, J. Role of Electrostatic Correlations in Polyelectrolyte Charge Association. *J. Chem. Phys.* **2018**, *149*, No. 163335.
(35) Agazzi, M. L.; Herrera, S. E.; Cortez, M. L.; Marmisollé, W. A.; Tagliazucchi, M.; Azzaroni, O. Insulin Delivery from Glucose-Responsive, Self-Assembled, Polyamine Nanoparticles: Smart "Sense-and-Treat" Nanocarriers Made Easy. *Chem. - Eur. J.* **2020**, *26*, 2456−2463.
(36) Smokers, I. B. A.; van Haren, M. H. I.; Lu, T.; Spruijt, E. Complex Coacervation and Compartmentalized Conversion of Prebiotically Relevant Metabolites. *ChemSystemsChem* **2022**, *4*, No. e202200004.
(37) Cakmak, F. P.; Choi, S.; Meyer, M. O.; Bevilacqua, P. C.; Keating, C. D. Prebiotically-Relevant Low Polyion Multivalency Can Improve Functionality of Membraneless Compartments. *Nat. Commun.* **2020**, *11*, No. 5949.
(38) Herrera, S. E.; Agazzi, M. L.; Cortez, M. L.; Marmisollé, W. A.; Tagliazucchi, M.; Azzaroni, O. Multitasking Polyamine/Ferrioxalate Nano-Sized Assemblies: Thermo-, Photo-, and Redox-Responsive Soft Materials Made Easy. *Chem. Commun.* **2019**, *55*, 14653−14656.
(39) Agazzi, M. L.; Herrera, S. E.; Cortez, M. L.; Marmisollé, W. A.; Azzaroni, O. Self-Assembled Peptide Dendrigraft Supraparticles with Potential Application in PH/Enzyme-Triggered Multistage Drug Release. *Colloids Surf., B* **2020**, *190*, No. 110895.
(40) Yewdall, N. A.; André, A. A. M.; Lu, T.; Spruijt, E. Coacervates as Models of Membraneless Organelles. *Curr. Opin. Colloid Interface Sci.* **2021**, *52*, No. 101416.
(41) Herrera, S. E.; Agazzi, M. L.; Cortez, M. L.; Marmisollé, W. A.; Tagliazucchi, M.; Azzaroni, O. Redox-Active Polyamine-Salt Aggregates as Multistimuli-Responsive Soft Nanoparticles. *Phys. Chem. Chem. Phys.* **2020**, *22*, 7440−7450.
(42) Wang, J.; Abbas, M.; Wang, J.; Spruijt, E. Selective Amide Bond Formation in Redox-Active Coacervate Protocells *ChemRxiv* 2021, DOI: 10.33774/chemrxiv-2021-1zt9k.
(43) Debais, G.; Tagliazucchi, M. Microphase Separation and Aggregate Self-Assembly in Brushes of Oppositely Charged Polyelectrolytes Triggered by Ion Pairing. *J. Chem. Phys.* **2020**, *153*, No. 144903.
(44) Martinez, M.; Pitarque, M.-A.; van Eldik, R. Outer-Sphere Redox Reactions in Sterically Hindered Pentaam(m)Inecobalt(III) Complexes. A Temperature and Pressure Dependence Kinetic Study. *J. Chem. Soc., Dalton Trans.* **1994**, 3159−3163.
(45) Zaldivar, G.; Tagliazucchi, M. Layer-by-Layer Self-Assembly of Polymers with Pairing Interactions. *ACS Macro Lett.* **2016**, *5*, 862−866.
(46) Vidyasagar, A.; Sung, C.; Gamble, R.; Lutkenhaus, J. L. Thermal Transitions in Dry and Hydrated Layer-by-Layer Assemblies Exhibiting Linear and Exponential Growth. *ACS Nano* **2012**, *6*, 6174−6184.
(47) Lutkenhaus, J. L.; McEnnis, K.; Hammond, P. T. Tuning the Glass Transition of and Ion Transport within Hydrogen-Bonded Layer-by-Layer Assemblies. *Macromolecules* **2007**, *40*, 8367−8373.
(48) Zhang, Y.; Batys, P.; O'Neal, J. T.; Li, F.; Sammalkorpi, M.; Lutkenhaus, J. L. Molecular Origin of the Glass Transition in Polyelectrolyte Assemblies. *ACS Cent. Sci.* **2018**, *4*, 638−644.
(49) Wang, Q.; Schlenoff, J. B. The Polyelectrolyte Complex/Coacervate Continuum. *Macromolecules* **2014**, *47*, 3108−3116.

(50) Perry, S. L.; Leon, L.; Hoffmann, K. Q.; Kade, M. J.; Priftis, D.; Black, K. A.; Wong, D.; Klein, R. A.; Pierce, C. F.; Margossian, K. O.; et al. Chirality-Selected Phase Behaviour in Ionic Polypeptide Complexes. *Nat. Commun.* **2015**, *6*, No. 6052.
(51) Nakashima, K.; Bahadur, P. Aggregation of Water-Soluble Block Copolymers in Aqueous Solutions: Recent Trends. *Adv. Colloid Interface Sci.* **2006**, *123*−*126*, 75−96.
(52) Banani, S. F.; Lee, H. O.; Hyman, A. A.; Rosen, M. K. Biomolecular Condensates: Organizers of Cellular Biochemistry. *Nat. Rev. Mol. Cell Biol.* **2017**, *18*, 285−298.
(53) Li, L.; Rumyantsev, A. M.; Srivastava, S.; Meng, S.; de Pablo, J. J.; Tirrell, M. V. Effect of Solvent Quality on the Phase Behavior of Polyelectrolyte Complexes. *Macromolecules* **2021**, *54*, 105−114.
(54) André, A. A. M.; Spruijt, E. Rigidity Rules in DNA Droplets: Nucleic Acid Flexibility Affects Model Membraneless Organelles. *Biophys. J.* **2018**, *115*, 1837−1839.
(55) Kokufuta, E. Colloid Titration Behavior of Poly-(Ethyleneimine). *Macromolecules* **1979**, *12*, 350−351.
(56) Koper, G. J. M.; Borkovec, M. Proton Binding by Linear, Branched, and Hyperbranched Polyelectrolytes. *Polymer* **2010**, *51*, 5649−5662.
(57) Choi, J.; Rubner, M. F. Influence of the Degree of Ionization on Weak Polyelectrolyte Multilayer Assembly. *Macromolecules* **2005**, *38*, 116−124.
(58) Besteman, K.; Van Eijk, K.; Lemay, S. G. Charge Inversion Accompanies DNA Condensation by Multivalent Ions. *Nat. Phys.* **2007**, *3*, 641−644.
(59) Delsanti, M.; Dalbiez, J. P.; Spalla, O.; Belloni, L.; Drifford, M. Phase Diagram of Polyelectrolyte Solutions in Presence of Multivalent Salts. In *Macro-Ion Characterization*; Schmitz, K. S., Ed.; American Chemical Society, 1993; pp 381−392.
(60) Sabbagh, I.; Delsanti, M. Solubility of Highly Charged Anionic Polyelectrolytes in Presence of Multivalent Cations: Specific Interaction Effect. *Eur. Phys. J. E - Soft Matter* **2000**, *1*, 75−86.
(61) Solis, F. J.; de la Cruz, M. O. Collapse of Flexible Polyelectrolytes in Multivalent Salt Solutions. *J. Chem. Phys.* **2000**, *112*, 2030−2035.
(62) Lytle, T. K.; Sing, C. E. Transfer Matrix Theory of Polymer Complex Coacervation. *Soft Matter* **2017**, *13*, 7001−7012.
(63) Perry, S. L.; Sing, C. E. PRISM-Based Theory of Complex Coacervation: Excluded Volume versus Chain Correlation. *Macromolecules* **2015**, *48*, 5040−5053.
(64) Wang, H.; Sayed, S. Y.; Luber, E. J.; Olsen, B. C.; Shirurkar, S. M.; Venkatakrishnan, S.; Tefashe, U. M.; Farquhar, A. K.; Smotkin, E. S.; McCreery, R. L.; Buriak, J. M. Redox Flow Batteries: How to Determine Electrochemical Kinetic Parameters. *ACS Nano* **2020**, *14*, 2575−2584.
(65) Izquierdo, J.; Kranz, C. Electrochemical Techniques for Investigating Redox Active Macromolecules. *Eur. Polym. J.* **2016**, *83*, 428−449.
(66) Yamada, H.; Yoshii, K.; Asahi, M.; Chiku, M.; Kitazumi, Y. Cyclic Voltammetry Part 1: Fundamentals. *Electrochemistry* **2022**, *90*, 102005.
(67) Muhammad, H.; Tahiri, I. A.; Muhammad, M.; Masood, Z.; Versiani, M. A.; Khaliq, O.; Latif, M.; Hanif, M. A Comprehensive Heterogeneous Electron Transfer Rate Constant Evaluation of Dissolved Oxygen in DMSO at Glassy Carbon Electrode Measured by Different Electrochemical Methods. *J. Electroanal. Chem.* **2016**, *775*, 157−162.
(68) Nicholson, R. S. Theory and Application of Cyclic Voltammetry for Measurement of Electrode Reaction Kinetics. *Anal. Chem.* **1965**, *37*, 1351−1355.
(69) Liu, Y.; Winter, H. H.; Perry, S. L. Linear Viscoelasticity of Complex Coacervates. *Adv. Colloid Interface Sci.* **2017**, *239*, 46−60.
(70) Spruijt, E.; Stuart, M. A. C.; van der Gucht, J. Linear Viscoelasticity of Polyelectrolyte Complex Coacervates. *Macromolecules* **2013**, *46*, 1633−1641.
(71) Moldenhauer, J.; Meier, M.; Paul, D. W. Rapid and Direct Determination of Diffusion Coefficients Using Microelectrode Arrays. *J. Electrochem. Soc.* **2016**, *163*, H672−H678.
(72) Iamprasertkun, P.; Ejigu, A.; Dryfe, R. A. W. Understanding the Electrochemistry of "Water-in-Salt" Electrolytes: Basal Plane Highly Ordered Pyrolytic Graphite as a Model System. *Chem. Sci.* **2020**, *11*, 6978−6989.
(73) Farhat, T. R.; Schlenoff, J. B. Doping-Controlled Ion Diffusion in Polyelectrolyte Multilayers: Mass Transport in Reluctant Exchangers. *J. Am. Chem. Soc.* **2003**, *125*, 4627−4636.

https://doi.org/10.1021/acs.jpcb.3c03680
J. Phys. Chem. B 2023, 127, 7636−7647